



RESEARCH ARTICLE

10.1029/2020JB019487

Key Points:

- At low temperature and pressure, chlorite is weak and velocity-strengthening and hornblende and epidote are strong and velocity-weakening
- Increasing chlorite content leads to mixtures becoming frictionally weaker and velocity-strengthening
- Striations correlate with weak and stable sliding, likely related to chlorite surface properties and slow growth of long contact asperities

Supporting Information:

- Supporting Information S1
- Table S1

Correspondence to:

Åke Fagereng,
fagerenga@cardiff.ac.uk

Citation:

Fagereng, Åke, & Ikari, M. J. (2020). Low-temperature frictional characteristics of chlorite-epidote-amphibole assemblages: Implications for strength and seismic style of retrograde fault zones. *Journal of Geophysical Research: Solid Earth*, 125, e2020JB019487. <https://doi.org/10.1029/2020JB019487>

Received 30 JAN 2020

Accepted 2 APR 2020

Accepted article online 8 APR 2020

Low-Temperature Frictional Characteristics of Chlorite-Epidote-Amphibole Assemblages: Implications for Strength and Seismic Style of Retrograde Fault Zones

Åke Fagereng¹  and Matt J. Ikari² 

¹School of Earth and Ocean Sciences, Cardiff University, Cardiff, UK, ²MARUM Research Faculty and Faculty of Geosciences, University of Bremen, Bremen, Germany

Abstract In retrograde faults exhuming mafic rocks, shearing occurs in metamorphic and/or hydrothermally altered mineral assemblages whose frictional properties are not well known. Here, we present the results of laboratory shearing experiments on chlorite schist, epidotite, and hornblende-dominated amphibolite and mixtures of these rocks and evaluate their frictional properties and microstructures. The experiments were conducted on powdered rock samples with starting grain size of <125 μm, at room temperature, under fluid-saturated conditions and applied normal stress of 10 MPa. The results show that chlorite schist is relatively weak (friction coefficient of 0.36), whereas epidotite and amphibolite are strong (friction coefficients of 0.63 and 0.67, respectively). The friction of chlorite schist-epidotite and chlorite schist-amphibolite mixtures decreases nearly linearly with increasing chlorite content. Chlorite schist exhibits velocity-strengthening behavior, epidotite is velocity-weakening, and the amphibolite shows mostly velocity-weakening friction. Mixtures show intermediate strength and velocity dependence of friction. Well-developed striations formed on slip surfaces in samples with ≥50% chlorite schist. The epidotite slip surface exhibits a mixture of very fine particles and coarser crystals. Amphibolite slip surfaces have less very fine grains and are composed of subhedral to euhedral needles. Few intragranular fractures are preserved, and we infer wear at contact asperities to be the likely cause of velocity-weakening in our epidote gouges. Addition of chlorite to epidotite and amphibolite produces a striated slip surface and disrupts contacts between harder grains. Therefore, retrograde chlorite growth is expected to facilitate frictional weakening and stable slip in higher-grade mineral assemblages exhumed to low-temperature conditions.

1. Introduction

The largest earthquakes generally nucleate near the base of the seismogenic zone, under greenschist facies conditions (e.g., Jiang & Lapusta, 2017; Sibson, 1982). Greenschist to amphibolite facies mineral assemblages, formed near the base of the seismogenic zone, may also host active shearing at shallower depths by exhumation through uplift and/or erosion (e.g., Abers et al., 1997; Norris & Cooper, 2007; Taylor et al., 2000). During exhumation, the mineral assemblage may be modified and weakened by fluid influx and retrogressive reactions (e.g., Diener et al., 2016; Holdsworth et al., 2011; Jefferies et al., 2006; Jiménez-Millán et al., 2015; Richard et al., 2014; Wintsch et al., 1995).

Consider a fault zone where the fault zone rocks include ferromagnesian minerals that experience exhumation and cooling from the base of the seismogenic zone to shallower conditions during progressive deformation. When cooling from amphibolite or greenschist to lower metamorphic facies, the amphibole species hornblende breaks down to chlorite and epidote, and to the amphibole species actinolite, if free water is present (e.g., Apter & Liou, 1983; Fagereng & Diener, 2011; Miyashiro, 1968). Therefore, faults exhuming greenschist to amphibolite facies mafic rocks can experience changes in frictional properties as mineral proportions change with increasing retrograde chlorite (+/− epidote) growth. However, in the absence of free water, faults can also accommodate exhumation of an existing amphibole-chlorite-epidotite assemblage. The proportion of chlorite may govern fault strength (e.g., Diener et al., 2016; Imber et al., 1997; Jiménez-Millán et al., 2015), and increased chlorite content has also been associated with a preference for aseismic creep rather than earthquake slip (Schleicher et al., 2012). Therefore, if the bulk rock composition is suitable for

©2020. The Authors.

This is an open access article under the terms of the Creative Commons Attribution License, which permits use, distribution and reproduction in any medium, provided the original work is properly cited.

chlorite growth, the extent of retrograde hydration may govern chlorite content and therefore frictional behavior (cf. Fagereng & Diener, 2011; Schleicher et al., 2012; Wintsch et al., 1995). Questions that consequently arise are as follows: (1) How strong is the influence of chlorite content? (2) When exhumed to shallow, seismogenic levels, what are the potential frictional behaviors of retrogressive fault zones? and (3) Are these frictional behaviors associated with specific microstructures?

Here, we first briefly review the rock record of chlorite-amphibole-epidote-bearing faults, and then present the results of laboratory shearing experiments on chlorite, epidote, and hornblende-rich rocks and mixtures thereof, to evaluate the frictional properties of these mineral assemblages. We recognize that other minerals, particularly albite and quartz, are also present in natural examples of retrograde fault zones. However, frictional properties for quartz- and feldspar-dominated materials have already been extensively studied (e.g., Blanpied et al., 1998; Ikari et al., 2011; Marone et al., 1990; Scruggs & Tullis, 1998; Shimamoto & Logan, 1981a), and we focus on faults accommodating exhumation of mafic rocks or faults where chlorite growth has occurred within the fault rock assemblage. The aims of these experiments are to (1) determine the frictional properties of chlorite, epidote, and amphibole; (2) explore the variation in frictional properties as a function of chlorite content; (3) use the experimental results to discuss the seismic behavior of faults exhuming mafic rocks; and (4) compare and contrast the structure of these faults to those active within quartzofeldspathic rocks.

1.1. Examples of Retrograde Faults

Retrograde phyllosilicate growth has been proposed to cause frictional weakening and a transition from seismogenic slip to aseismic creep (e.g., Wintsch et al., 1995). On the transpressional Alpine Fault in New Zealand, greenschist to amphibolite-facies rocks are exposed at the surface but contain recent slip surfaces localized in a phyllosilicate-rich fault gouge (Norris & Cooper, 2007). The Alpine fault Deep Fault Drilling Project Phase 1 documented a tens of meters thick, mostly cataclastic fault core containing centimeter-scale principal slip zones, at a depth of <150 m below the surface (Toy et al., 2015). Although this gouge is compositionally and structurally compatible with near-surface fault creep (Barth et al., 2013), such creep is not observed and the gouge may be velocity-weakening at higher temperatures and pressures (Boulton et al., 2014; Ikari et al., 2015; Niemeijer et al., 2016). These studies suggest a time-dependent evolution, where Alpine fault rocks record progressive alteration of the greenschist to amphibolite protolith and a complicated deformation history (Toy et al., 2015). Time-dependent behavior coupled to retrograde phyllosilicate growth is also indicated by faults in the Woodlark Basin, near Papua New Guinea. There, scientific drilling during Ocean Drilling Project Leg 180 recovered core samples from Site 1117 on the Moresby Seamount, interpreted to be exhumed by detachment normal faulting (Taylor et al., 2000; Taylor & Huchon, 2002). Samples revealed a chlorite-talc-serpentine-carbonate fault gouge derived from a quartz-epidote-chlorite protolith. On the San Andreas Fault, Schleicher et al. (2012) proposed that the degree of smectite-chlorite neomineralization, controlled by fracture and fluid infiltration, may control locations of fault creep. Fagereng and Diener (2011) similarly suggested that retrogressive mineral reactions moderated by limited and localized fluid infiltration may be a control on San Andreas Fault slip behavior.

Near-surface, well-preserved exposures or core samples of active faults as those described above are rare and commonly difficult to interpret. However, exhumed faults commonly expose variably altered amphibolite to greenschist facies fault rocks (Figure 1). For example, reports from the Outer Hebrides fault zone (e.g., Imber et al., 1997) and the Moine thrust at Loch Eriboll (e.g., McClay & Coward, 1981; Read, 1934), both in Scotland, describe retrograde growth of chlorite as a major control on strain localization and fault zone weakening. In the Outer Hebrides fault zone, deformation is concentrated in chloritic shear zones, where chlorite foliation wraps around more competent quartzofeldspathic rocks (Figure 1a; Imber et al., 1997, 2001). These macroscopically ductile shear zones locally overprint brittle faults, in a brittle-to-ductile transition inferred to be driven by retrogression and growth of phyllosilicates at constant temperature and pressure (Imber et al., 1997, 2001). Similarly, chlorite-epidote-quartz-albite mylonites of the Moine sequence include retrograde, lineated phyllonites with fractured epidote grains wrapped by chlorite foliation (Figures 1b and 1c; Evans & White, 1984; Holdsworth et al., 2007). At the base of the Kalak Nappe in the Norwegian Caledonides, retrograde deformation also occurs in relatively late stage well foliated chloritic layers, containing asymmetric, sheared clasts of stronger quartz (Figure 1d; Zwaan & Roberts, 1978). In all these major thrusts, the rocks show strain localization coupled to retrograde chlorite growth within a broad zone of



Figure 1. Examples of chlorite-bearing, exhumed faults. (a) Field exposure of the Outer Hebrides fault zone, with chloritic foliation wrapping around a quartzofeldspathic lens. (b) Exposure of chlorite-epidote schist in the Moine thrust zone, by Loch Eriboll, Scotland, with fractured epidote grains in a chloritic foliation visible at the microscale in cross-polarized light in (c). (d) Chlorite also defines the foliation at the base of the Kalak Nappe by Talvik, in the northern Norwegian Caledonides. (e) Chloritic foliations are not only restricted to retrograde faults but also form at prograde conditions in subduction thrusts, here represented by the Nishisonogi metamorphic rocks, Kyushu, Japan.

preexisting deformation. This localization can be a result of fluid-controlled replacement of strong phases. In the exhumed strike-slip Kuckaus Mylonite Zone, Namibia, Diener et al. (2016) suggest that chlorite growth by fluid-rock interactions allowed strain localization into centimeter-wide fault cores within a kilometer-wide deforming zone. Replacement of load-bearing strong phases with weak phyllosilicates as a consequence of cataclasis and alteration was also described in the Median Tectonic Line of Japan (Jefferies et al., 2006). While we focus here on retrograde structures, we also note that deformation localization within chloritic shear zones is also seen in subduction-related thrusts, such as in the Nishisonogi metamorphic rocks of Japan, where chloritic shear zones developed on the prograde path contain fractured clasts of amphibole and feldspar (Figure 1e; Mori et al., 2014).

All the deformation zones described above show evidence for strain localization into relatively narrow zones containing chlorite, epidote, and amphibole (and possibly white micas, quartz and feldspar). This observation implies that these minerals likely play an important role in governing fault behavior in several settings; however, little is known of their frictional properties, providing a rationale for our current study. One hypothesis is that the extent of chlorite growth is critical for fault zone strength and slip behavior (Fagereng & Diener, 2011; Imber et al., 1997; Schleicher et al., 2012; Wintsch et al., 1995), which we evaluate for near-surface faults with laboratory shearing experiments.

2. Materials and Methods

We obtained separate rock samples of epidotite, amphibolite, and chlorite schist (all from Ward's Natural Science), individually rich in the minerals epidote, hornblende, and chlorite, respectively (Figure 2a). Semiquantitative mineral assemblages were determined by X-ray diffraction patterns measured on a Philips X'Pert Pro multipurpose diffractometer at the Faculty of Geosciences, University of Bremen (Vogt et al., 2002) and interpreted with the software PANalytical HighScore™. Our chlorite schist sample is composed of 96% chlorite; our epidotite sample is composed of 69% epidote, 20% amphibole (pargasite), and 11% sphene; and our amphibolite sample contains 89% hornblende, with minor amounts of quartz, feldspar, and phlogopite.

The samples were powdered by hand with a mortar and pestle to a grain size of <125 μm. The powders were mixed with demineralized water and pressed into a shear cell, which consists of a stack of two metal plates having an empty cylindrical sample volume of 25 mm diameter and up to ~20 mm height. This sample preparation produces a random initial distribution of grain sizes, shapes, and compositions. The cell is loaded

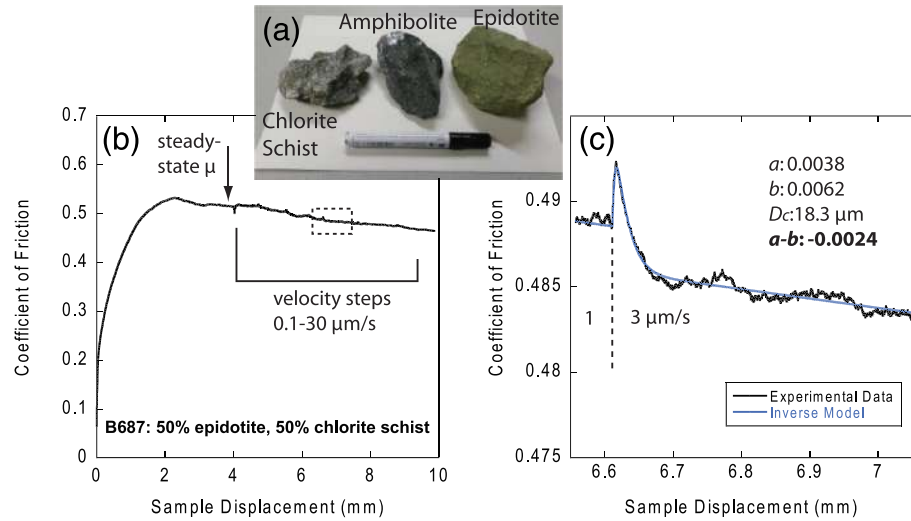


Figure 2. (a) Starting materials for this study: chlorite-, hornblende-, and epidote-rich rock samples. (b) Example of a friction-displacement curve, showing the measurement of the steady-state residual value μ and a velocity-step sequence. (c) Individual velocity step shown in (b) with experimental data overlain by an inverse model, with parameters listed.

into a single-direct shear device at Marum Research Faculty at the University of Bremen, Germany. This apparatus induces planar shear by displacing the plates relative to each other. This configuration enforces deformation localization onto a thin (<1 mm; section 3.2), horizontal zone in the center of the sample. All experiments were conducted at room temperature, saturated with deionized water and under an applied normal stress of 10 MPa. After application of the normal stress, the samples are allowed to consolidate for at least 18 hr, sometimes up to 2 days, in order to allow excess fluid drainage. Shearing tests are conducted after the sample height change becomes negligible, so that any excess pore pressure is assumed dissipated and therefore that the applied normal stress is the effective normal stress σ_n' (for further details see Ikari et al., 2015, online version). We employ an initial constant displacement rate of 10 $\mu\text{m/s}$ in order to establish steady-state shear strength τ , typically measured at $\sim 4\text{--}5$ mm displacement (Figure 2b). In some cases, steady state was not reached within 5 mm; in these cases we measure the shear strength at 5 mm for comparison between experiments. We calculate a residual sliding coefficient as $\mu = \tau/\sigma_n'$, assuming that our sheared samples are cohesionless, but note that this may not necessarily be the case for samples with a high clay mineral content (Ikari & Kopf, 2011).

After a displacement of ~ 5 mm and measurement of residual frictional strength, we employed stepwise threefold increases in the sliding velocity (V) in the range 0.1–30 $\mu\text{m/s}$. From these tests, we quantify the slip rate dependence of friction by the parameter $a-b = \Delta\mu/\Delta\ln V$, where $\Delta\mu$ is the difference between an initial steady-state friction value μ_0 at a reference velocity V_0 and a new steady-state friction value μ at the new velocity V (e.g., Dieterich, 1981; Marone, 1998). Although the parameter $a-b$ can be calculated by directly measuring $\Delta\mu$, we employ a more rigorous method considering the frictional response to a velocity step as follows:

$$\mu = \mu_0 + a \ln\left(\frac{V}{V_0}\right) + b_1 \ln\left(\frac{V_0 \theta_1}{D_{c1}}\right) + b_2 \ln\left(\frac{V_0 \theta_2}{D_{c2}}\right) \quad (1)$$

$$\frac{d\theta_i}{dt} = 1 - \frac{V\theta_i}{D_{ci}}, \quad i = 1, 2 \quad (2)$$

where a , b_1 , and b_2 are dimensionless constants, θ_1 and θ_2 are state variables which describe aging, and D_{c1} and D_{c2} are critical slip distances over which friction evolves to a new steady-state value (Blanpied et al., 1998; Dieterich, 1981; Marone, 1998). In cases where the data are well described by a single-state variable, we take $D_{c1} = D_{c2}$ and $b_2 = 0$. Equation 2 describes the evolution of friction to steady state at the new velocity V and is known as the Dieterich law, which explicitly considers that friction can evolve as a function

of time and not necessarily slip (Dieterich & Kilgore, 1994). We determine the individual parameters a , b_1 , b_2 , D_{c1} , and D_{c2} from a fifth-order Runge-Kutta numerical integration that also includes an expression for finite system stiffness and an inverse solution using an iterative least squares method (Figure 2c) (e.g., Blanpied et al., 1998; Ikari et al., 2009; Reinen & Weeks, 1993; Saffer & Marone, 2003).

We report $a-b$, where $b = b_1 + b_2$ to account for the possibility of one state variable or two state variables. This parameter is critical for predicting fault slip behavior, because frictional instability on faults that results in seismic slip requires a strength loss in response to a slip rate increase (i.e. velocity-weakening friction) or $a-b < 0$ (e.g., Dieterich, 1986; Dieterich & Kilgore, 1996; Scholz, 1998). Velocity-strengthening friction ($a-b > 0$) favors aseismic slip. Velocity-weakening friction is an indicator of potential slip instability, but the appearance of unstable slip, as earthquakes on natural faults and stick-slip behavior in the laboratory, requires sufficiently low elastic stiffness in the fault surroundings (the wall rock on natural faults and the testing apparatus in the laboratory) (Cook, 1981; Scholz, 1998). Changes in friction slip-dependence during velocity steps can also influence frictional stability (e.g., Ito & Ikari, 2015); however, we removed long-term slip-weakening or slip-hardening trends from each individual velocity step to isolate the purely velocity-dependent component of the friction change (e.g., Blanpied et al., 1998).

Two sets of experiments were performed, based on postexperiment imaging goals. For the first set a reduced sample volume was utilized, designed so that the sample height was targeted to be ~ 7 – 8 mm under normal load, with the shear surface located ~ 2 – 3 mm below the top of the sample. These samples were set in epoxy after shearing to analyze the slip surfaces in cross-section view. The samples were cut with a rock saw perpendicular to the slip surface and parallel to the slip vector. Backscattered scanning electron images were acquired using a Philips/FEI-XL30 field emission gun environmental scanning electron microscope (SEM) in the School of Earth and Ocean Sciences, Cardiff University. The SEM was operated in high vacuum mode with an accelerating voltage of 20 kV and a 50 μm diameter aperture.

For the second set of experiments, the full sample cell volume was loaded with water-saturated powders so that the sample consolidated to ~ 18 – 21 mm, with the shear surface being approximately midway through the sample. For these experiments a Poisson effect from the normal load induces a lateral force from the sample onto the side walls of the sample cell. This effect allows the sample halves to be separated along the shear surface upon removal from the experimental assembly, to reveal distinct slip surface textures for each sample. The sheared sample surfaces were immediately photographed and subsequently studied in detail. These samples were imaged normal to the slip surface with the SEM in low vacuum mode (0.5 Torr maintained using H_2O vapor), accelerating voltage of 20 kV, and 30 μm diameter final aperture. For some of these larger height samples, the Poisson effect causes a nonnegligible shear resistance between the sample and the cell walls, so that the full normal load is not transmitted to the shear surface. This is identifiable by a clear reduction in shear stress compared to the shorter samples for which this effect is minimal due to the small contact area with the side walls above the shear surface. In the cases where the reduction in normal stress was estimated to be larger than 5%, the samples were used for imaging only and the mechanical data are excluded (Table S1 in the supporting information).

Grain size distributions for slip surfaces developed in the end-member rock samples were obtained from backscatter scanning electron images taken normal to the slip surfaces, using ImageJ software (available from <https://imagej.nih.gov/ij/>) and Jazy macros created by Rüdiger Kilian (downloaded from https://github.com/kilir/Jazy_macros). The workflow for image segmentation follows Heilbronner (2000). After segmentation, we fit ellipses to grains to obtain their long and short axis lengths and define grain size as the geometrical mean of these lengths (e.g., Shimamoto & Nagahama, 1992). We also use these data to quantify shape-preferred orientations (e.g., Cladouhos, 1999), defined by the orientation of grain long axes measured as an angle from -90° to $+90^\circ$ from the slip direction. For mixtures, we describe grain sizes and shapes qualitatively with reference to the end-member analyses.

3. Results

3.1. Frictional Properties

Epidotite, amphibolite, and epidotite-chlorite schist mixtures with 50% and 70% epidotite and the ternary epidotite-amphibolite-chlorite schist mixture are frictionally strong with residual μ values ranging from

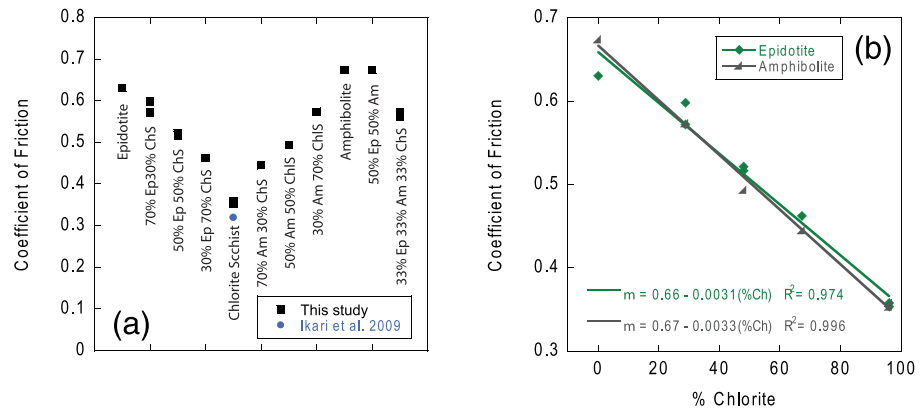


Figure 3. (a) Residual coefficient of friction for all samples in this study. Data from Ikari et al. (2009) for the same chlorite schist sample shown for comparison. (b) Linear mixing laws for epidote and hornblende as a function of chlorite content. Am = amphibolite, Ep = epidotite, ChS = chlorite schist.

0.52 to 0.67 (Figure 3a and Table S1). Chlorite schist is the weakest sample, having a residual coefficient of friction μ of 0.36. Mixtures of epidotite-chlorite schist and amphibolite-chlorite schist form nearly identical linear mixing lines (Figure 3b). The chlorite schist value from this study is similar to the value of 0.32 measured by Ikari et al. (2009) for the same sample under similar conditions (room temperature, water saturated, 12 MPa effective normal stress).

Results of inverse modeling show that the velocity-dependence of friction exhibits a mixture of positive and negative values for all samples containing hornblende, with $a-b$ ranging from -0.015 to 0.004 (Figure 4a and Table S2). Epidotite and the mixture of 70% epidotite and 30% chlorite schist are velocity-weakening and exhibit $a-b$ of -0.007 to near zero. Chlorite schist is velocity-strengthening under our testing conditions ($a-b$ of 0.001 to 0.013). For mixtures of chlorite schist with epidotite or amphibolite, $a-b$ values increase with increasing chlorite content. For chlorite schist, $a-b$ clearly increases with sliding velocity; however, this trend is weak to nonexistent for all other samples in this study (Figure S1). The velocity-dependent frictional behavior of chlorite schist, including the range of $a-b$ values and the positive dependence of $a-b$ on slip velocity, is consistent with the results of Ikari et al. (2009). In summary, epidotite is velocity-weakening, amphibolite is mostly velocity-weakening, and chlorite schist is velocity-strengthening, and in mixtures over 50% chlorite schist is necessary for primarily velocity-strengthening friction. Samples containing hornblende can be either velocity-weakening or velocity-strengthening but tend to have greater $a-b$ if there is more chlorite

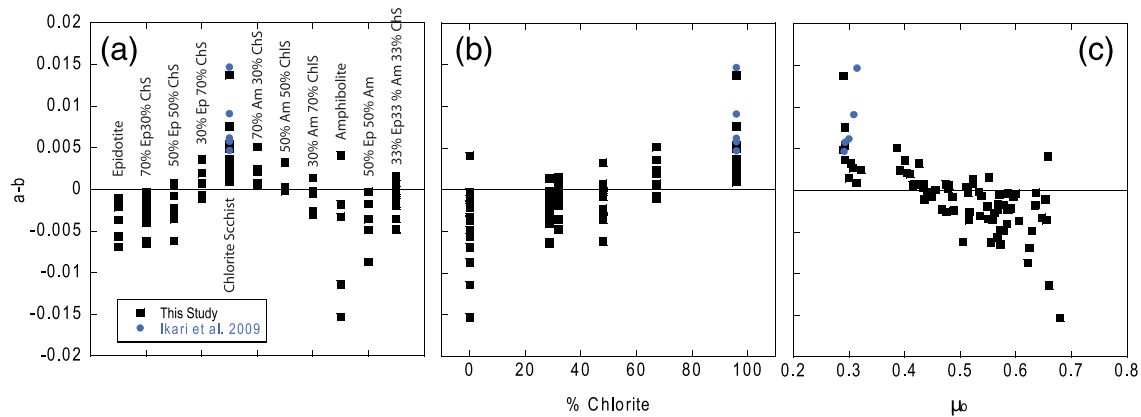


Figure 4. Velocity-dependent friction parameters for all samples in this study. (a) $a-b$ values for all samples and velocity steps. (b) Plot of $a-b$ against the proportion of chlorite in the sample. (c) Plot showing a general decrease in $a-b$ with increasing initial steady-state friction. Data from Ikari et al. (2009) for the same chlorite schist sample shown for comparison. Am = amphibolite, Ep = epidotite, ChS = chlorite schist.

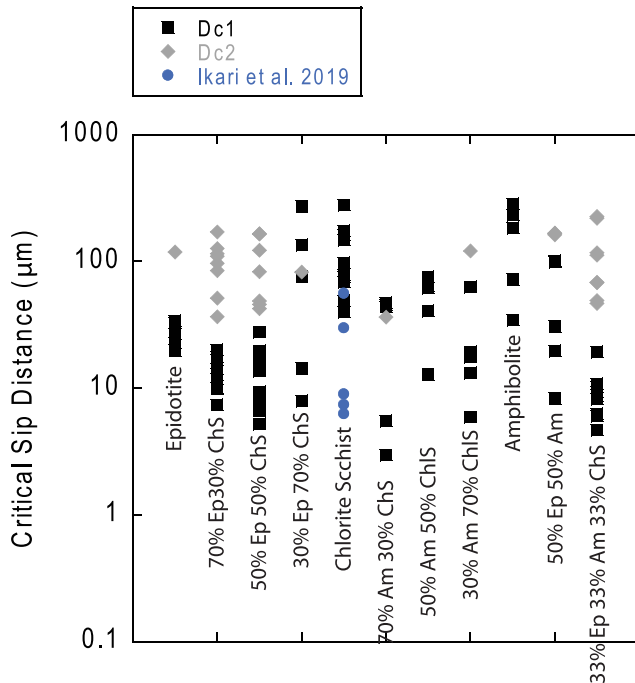


Figure 5. Critical slip distance (D_c) determined from velocity-step tests. Data from Ikari et al. (2009) for the same chlorite schist sample shown for comparison. Where required for a good model fit, two D_c (D_{c1} and D_{c2}) values were determined. Am = amphibolite, Ep = epidotite, ChS = chlorite schist.

present. These patterns are also reflected in an overall increase in $a-b$ with increasing chlorite content (Figure 4b) and a general decrease in $a-b$ with increasing initial steady-state friction (Figure 4c).

The inverse modeling was also used to derive the critical slip distance (D_c) for each experiment (Figure 5). Although there is significant scatter in the data, D_c is longer for the chlorite schist (40–278 μm) and amphibolite (34–285 μm) end-members than the epidotite (20–33 μm). The mixtures are more complex and tend to require two D_c values to fit the data; however, consistent with longer D_c in chlorite, the 70% chlorite schist sample exhibits larger D_c , or D_{c1} , compared to samples with more epidote (Figure 5). Mixtures of amphibolite and chlorite schist tend to have lower D_c or D_{c1} values compared to the end-members.

3.2. Microstructures

The experimental setup localizes strain onto a well-defined, few 100 μm thick, planar zone, along which we separated the sample upon completion of a subset of our experiments. Postexperiment photographs of these shear surfaces show that the end-member amphibolite and epidotite samples have a relatively rough texture at the millimeter scale, with little to no shape-preferred orientation (Figure 6). Chlorite schist, on the other hand, exhibits well-developed striations aligned with the shearing direction. Less well developed striations are observed for mixtures with 50% or more chlorite. Note that we define “striations” following Toy et al. (2017), as linear grooves or slickenlines on the slip surface, typically inferred to result from brittle wear (e.g., Engelder, 1974; Hancock, 1985; Petit, 1987).

SEM backscatter electron images of the slip surfaces show that the epidotite developed a gouge with some larger ($\leq 100 \mu\text{m}$) clasts in a very fine, down to submicrometer grain-sized matrix but no shape-preferred alignment of grain long axes (Figures 7a, 7b, 8a, and 8b). The chlorite schist sample has a striated slip surface, where the striations appear as linear, mechanical wear features along the surface, but these lines are also associated with fine chlorite grains (Figures 7c, 7d, and 8c). A few grains are elongated and oriented subparallel to the striations



Figure 6. Photographs of sample shear surfaces, taken immediately after the experiments. The cylindrical samples are 25.4 mm in diameter. Backscatter scanning electron images in Figures 7 and 9 were obtained looking normal to slip surfaces like those seen here. Such images cover areas of highest displacement, as on the left-hand side on each of these photographed surfaces.

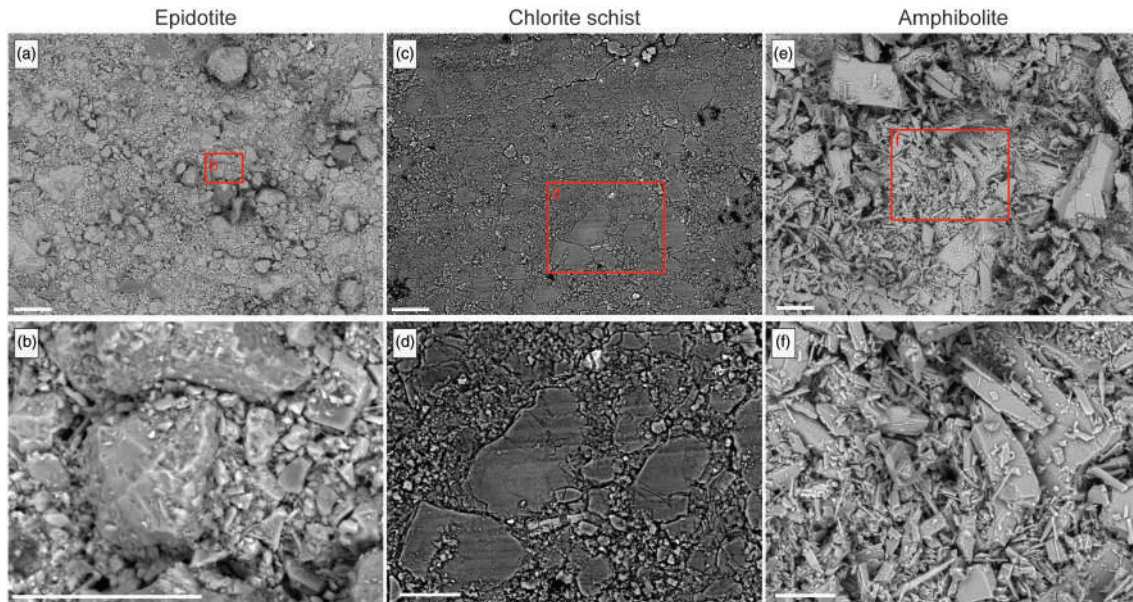


Figure 7. Backscatter scanning electron images of recovered slip surfaces of end-member samples. The view is normal to the slip surface, and shear sense is horizontal, nearside toward the left. (a, b) Epidotite with relatively equant grains and a grain size range from submicrometer (fine grains in b) to tens of micrometer. (c, d) Chlorite schist, where striations (subhorizontal in the sample view) are defined by grooves and very fine grains. (e, f) Amphibolite, lacking striations, but composed of subhedral to euhedral needles from a few μm to $>100 \mu\text{m}$ in length. In (a), (c), and (e) the scale bar is $100 \mu\text{m}$; in (b), (d), and (f) the scale bar is $50 \mu\text{m}$.

(Figure 8d). The amphibolite sample has a slip surface lacking striations (Figure 7e), but this slip surface also lacks the submicrometer, very fine grained material that is present on the slip surface in the epidotite and chlorite schist samples (Figures 7f and 8e). The amphibolite slip surface is better described as a mixture of

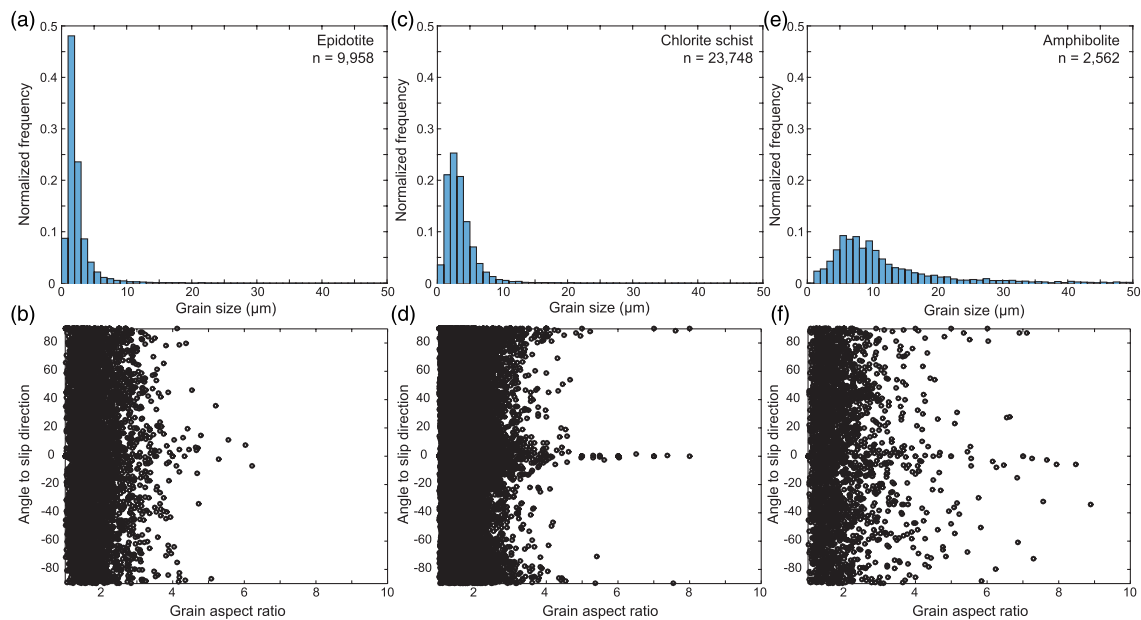


Figure 8. Grain size histograms and plots of grain orientation versus aspect ratio, based on image analysis of backscatter scanning electron images 8a, 8c, and 8e. Data for the epidotite (a, b) indicate that over half the grains are less than $2 \mu\text{m}$ in length and largely of low aspect ratio with scattered long axis orientations. About a quarter of the chlorite grains are $<2 \mu\text{m}$ (c), and in the chlorite schist a few larger aspect ratio grains are aligned with long axes parallel to the slip direction, but aspect ratios are low for most grains (d). The amphibolite has a greater range of grain sizes (e) and more large aspect ratio grains (f) than the other samples.

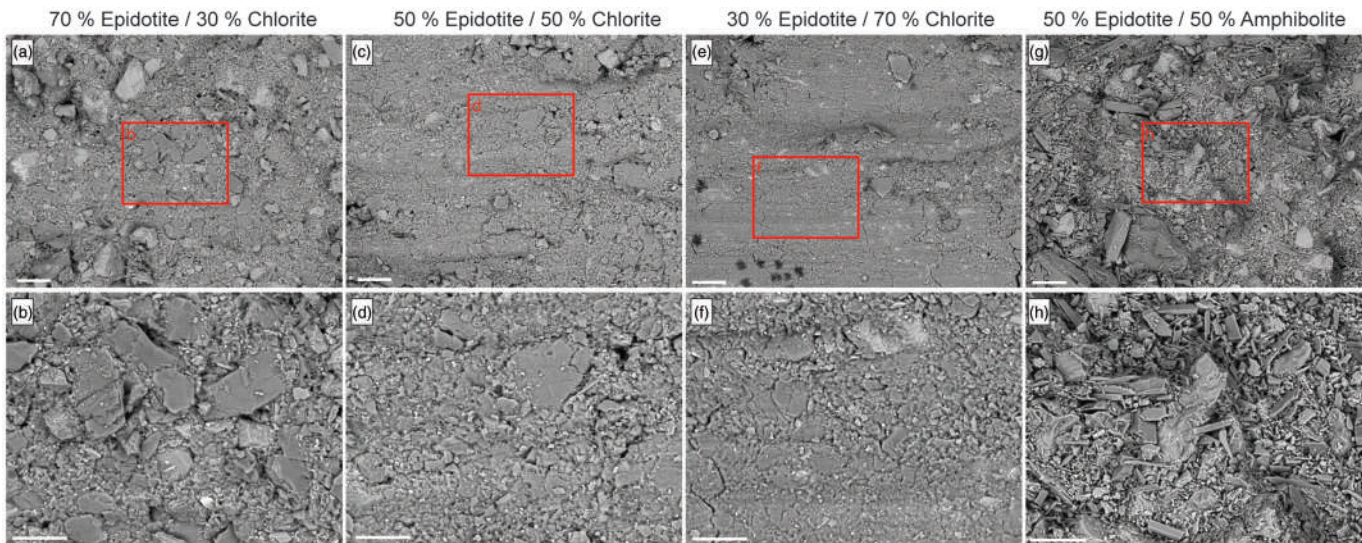


Figure 9. Backscatter scanning electron images of slip surfaces recovered from mixtures of epidotite and chlorite schist. The view is normal to the slip surface, and shear sense is horizontal, nearside toward the left. (a, b) A 70/30 mixture of epidote and chlorite schist; striations are poorly developed. (c, d) A 50/50 mixture of epidote and chlorite schist; grooves defining a striation are weakly developed. (e, f) A 30/70 mixture of epidote and chlorite schist, with well-developed striations on a slip surface largely coated by chlorite. (g, h) A 50/50 mixture of epidotite and amphibolite, where epidote grains (lighter shade) are generally equant and fragmented into smaller grains than the subhedral to euhedral amphibole needles (darker shade). In (a), (c), (e), and (g) the scale bar is 100 μm ; in (b), (d), (f), and (h) the scale bar is 50 μm .

subhedral to euhedral hornblende needles and prisms ranging in length from about 1 μm to over 100 μm (Figures 7f and 8e). These needles have scattered orientations (Figure 8f).

For the 70/30 mixture of epidotite/chlorite schist, the slip surface locally shows poorly defined striations, but neither chlorite nor epidote long axes show an alignment with these grooves (Figures 9a and 9b). Some very fine grained epidote, as developed on slip surfaces in the epidotite end-member (Figures 7a, 7b, and 8a), are present on these slip surfaces (Figure 9b). For the 50/50 epidotite/chlorite schist mixture there is more local striation development, and less fine grained epidote, compared to the 70/30 mixture (Figures 9c and 9d). For 30/70 epidotite/chlorite schist mixture, the striations are well developed (Figures 9e and 9f), although not as clear as in the chlorite schist end-member sample. Very little, if any, submicrometer epidote is visible. The 50/50 chlorite schist/amphibolite mixture, similar to the 50/50 epidotite/chlorite schist sample, has locally well developed striations.

The slip surface on the 50/50 epidotite/amphibolite sample is informative for the difference in behavior of amphibole and epidote at the laboratory shear conditions applied here. The amphibole forms needles of a range of sizes, with local intragranular fractures along cleavage planes (Figures 9g and 9h). Epidote, on the other hand, forms relatively equant shapes and no preserved intragranular fractures. This leads to a slip surface containing amphibole needles and generally low aspect ratio epidote grains in a fine matrix (Figures 9g and 9h).

From experiments where the sample was not separated along the shear surface, cross-section images show that the slip zone is an irregular zone a few 100 μm to 1 mm thick in the epidotite sample (Figure 10a) and a fracture-bound, few 100 μm thick zone for the mixture of 50% epidotite and 50% chlorite schist (Figure 10b). In these samples, coarse (<100 μm) epidote grains are present and surrounded by much finer grains in the epidotite end-member, whereas the mixture shows similar coarse epidote grains in a chlorite-rich matrix. A weakly developed foliation is present within the mixture but not in the epidotite. In the chlorite schist end-member, a localized, <100 μm thick, slip zone marks a boundary between chaotic and foliated chlorite above and a lack of foliation below (Figures 10c and 10d). Along the slip surface, well-oriented, slip surface-parallel chlorite grains are locally present (Figure 10d). A chaotic zone less than a millimeter thick separates the localized slip zone from overlying foliated chlorite (Figure 10c); this chaotic zone contains irregular open fractures that are roughly in the R-type shear surface orientation.

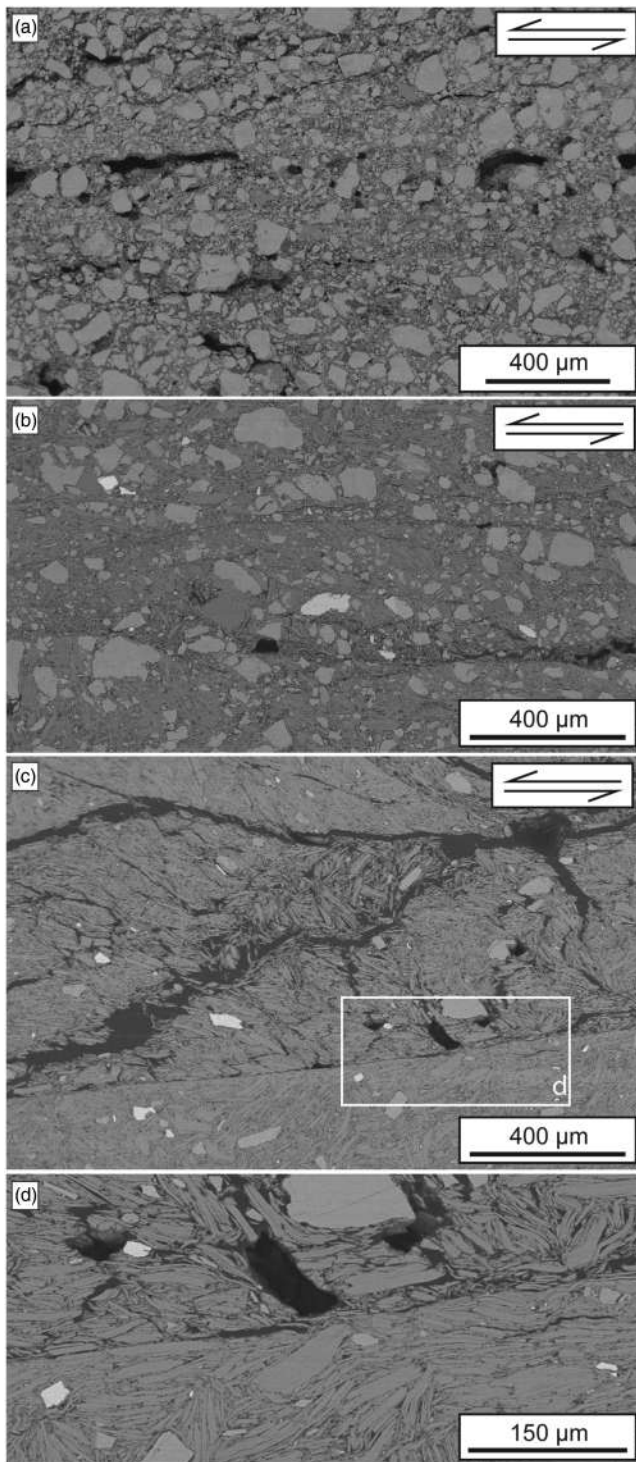


Figure 10. Backscatter scanning electron images of samples set in epoxy immediately after experiments and cut parallel to the slip direction and perpendicular to the slip surface: (a) Epidotite, (b) 50% epidotite and 50% chlorite schist, and (c, d) chlorite schist.

4. Discussion

4.1. Microstructural Controls on Frictional Behavior

The epidotite surface exhibits a large proportion of very fine particles in addition to coarser crystals (Figures 7a, 7b, and 8a), a feature also seen in cross section (Figure 10a). The amphibolite slip surface also contains a large range of grain sizes, but whereas the epidote grains are relatively equant, the hornblende forms needles at a range of sizes and aspect ratios (Figures 7e, 7f, 8e, and 8f). The epidotite slip surface is dominated by fine ($<2 \mu\text{m}$; Figures 7b and 8a) particles, including submicrometer grains that are not observed in the sheared amphibolite (Figures 7f and 10e). The mechanism of grain size reduction in epidotite, which rarely exhibits intragranular fractures in our experimental samples, is likely wear at micron- or submicron-scale asperity contacts, which produces the fine, anhedral particles while conserving the larger grains. The amphibolite, on the other hand, shows subhedral to euhedral, locally large aspect ratio hornblende needles, likely due to well-developed cleavage along which fractures can occur.

Weakening mechanisms leading to instability remain a central question in earthquake physics, and the specific mechanism may vary with deformation conditions, given the range of mechanisms that can operate at different temperature, stress, and fluid pressure conditions in various materials (e.g., Boutareaud et al., 2012; Di Toro et al., 2011; Scuderi et al., 2017; Segall & Rice, 2006). We focus here on the importance of plastic deformation of grain-to-grain contact asperities, which has been suggested from theoretical and experimental studies to control the rate-and-state dependence of friction (e.g., Baumberger & Caroli, 2006; Dieterich & Kilgore, 1994; Ikari et al., 2016; Sleep, 2005). Initially small real areas of contact, as is the case for strong framework minerals, are favorable for relatively rapid growth via plastic deformation; this is favorable for velocity-weakening because contact growth is limited at faster velocities, weakening the fault. Our epidotite gouge is characterized by several larger, equant grains (Figures 7a and 10a) and $>50\%$ very fine ($\leq 2 \mu\text{m}$) grains (Figure 8a), which suggests that fracturing preferentially occurs as wear at contact asperities creating fine particles and leaving larger crystals relatively intact. Therefore, we infer that deformation at these asperities plays a large role in controlling macroscopic frictional behavior and likely causes the consistent velocity-weakening in our epidote gouges. In contrast, the amphibolite shows a preference for fracturing along weak cleavage planes in hornblende. This leads to a needle-like grain shape and a grain size distribution including intermediate sizes not seen in the epidotites (Figures 7e and 8e). This may reduce the tendency for velocity-weakening friction by elongating the contact asperities. The variation in frictional stability of the amphibolite, with both positive and negative $a-b$ (Figure 4), may therefore be related to a specific distribution of grain shape and size controlled by cleavage planes. Sánchez-Roa et al. (2017) have also suggested a correlation between grain shape and behavior, where platy phyllosilicates are crystallographically favorable for weak and stable frictional behavior, relative to more fibrous phases of the same composition.

Chlorite is the frictionally weakest component in our samples (Figure 3a). By defining striated slip surface patches separated by relatively intact epidote and amphibole grains (Figure 9), chlorite appears to accommodate shear localization in the mixtures, as it also does in natural

faults (Figure 1). The chlorite schist also developed the most localized end-member slip zone (Figure 10). The linearity of the epidotite-chlorite schist and amphibolite-chlorite schist mixing trends (Figure 3b) indicates that the slip surface strength is proportional to the volume fraction of chlorite, similar to the observations of Shimamoto and Logan (1981b) for clay-anhydrite mixtures. This would imply that slip occurs within a thin gouge zone in the mixed material, and the frictional behavior is governed by the volume fraction of each mineral. This is consistent with the cross-section microstructures, where slip did not localize onto a chlorite dominated surface (or surfaces) in the chlorite-epidotite mixture (Figure 10b). Because our gouges have initially random grain orientations and mineral distribution, it is likely that the chlorite volume required for frictional weakening and stable sliding in the experiments is greater than in natural faults, where interconnected chlorite-rich layers may be locally present from either localized growth or primary layering in the protolith (Figure 1) (Imber et al., 1997; Shimamoto & Logan, 1981b), and where smearing of chlorite to enhance interconnectivity of weak surfaces may occur with increasing strain (Rutter et al., 2013).

Very fine ($<2 \mu\text{m}$) epidote grains are common in the epidotite slip surface but rare in the mixtures with at least 50% chlorite schist (Figures 9c–9f), suggesting that frictionally weak chlorite grains disrupt the epidote-epidotite contact asperities that we infer to generate very fine grains. If velocity-weakening friction is controlled by deformation at these asperities, the presence and absence of these fine epidote grains correlate with unstable and stable frictional behavior, respectively. This is consistent with the observed velocity-strengthening frictional behavior of samples with $>50\%$ chlorite (Figure 4b). Similarly, chlorite would also disrupt hornblende-hornblende contacts. Chlorite is clearly the weakest component of our samples, so the presence of chlorite which disrupts the contacts between stronger grains simultaneously results in overall frictional weakening. The tendency for frictional weakness to be associated with velocity-strengthening behavior (Figure 4c) is consistent with previous work on a wide range of natural and analog fault gouges (Beeler, 2007; Carpenter et al., 2011; Ikari et al., 2011, 2016; Morrow et al., 1992; Shimamoto & Logan, 1981b; Tesei et al., 2012). That increased chlorite content favors frictional stability is also consistent with hypotheses raised from studies of natural fault rocks (e.g., Imber et al., 1997; Schleicher et al., 2012; Smith & Faulkner, 2010).

4.2. Shear Surface Structure

Chlorite crystals appear to align and coat the slip surface where powdered chlorite schist makes up $\geq 50\%$ of the sample (Figures 10c and 10d), and in these experiments striations have also developed (Figures 7c and 7d and 9c–9f). Our interpretation is therefore that slip preferentially occurs on the weak chlorite, and strength is higher where other, stronger, minerals host shear. This is analogous to, but less pronounced than, through-going, polished, striated phyllosilicate surfaces that hosted localized deformation in clay-gouge experiments by Haines et al. (2013). They investigated fabric development in clay gouges and observed the formation of a zone of Riedel shears bounding phyllosilicates in the P-orientation, which flatten to lower angles and become undulatory at greater strains. This, and other experiments describing the microstructural development of slip zones with anastomosing phyllosilicate fabric, typically investigates a deforming material volume with a substantial nominal thickness (e.g., Colletini et al., 2009; Haines et al., 2013; Logan & Rauenzahn, 1987; Niemeijer & Spiers, 2005; Rutter et al., 1986; Scruggs & Tullis, 1998). We suggest that the experimental boundary conditions of our deformation apparatus favored rapid development of a localized slip surface in the chlorite schist end-member (Figures 10c and 10d), preserving none or a minor component of the Riedel shear-forming phase observed in the other studies.

The rough fault surfaces in velocity-weakening epidote and hornblende are clearly different from the smoother surfaces with slip-parallel striations in the velocity-strengthening chlorite (Figure 6). The striation development that occurred in the frictionally weak, stably sliding chlorite-rich samples suggests that lineations in fine-grained phyllosilicates may correlate with velocity-strengthening frictional behavior and therefore fault creep. Striations in montmorillonite have been observed previously in experiments at low temperatures ($\leq 80^\circ\text{C}$) but were absent at higher temperature conditions (Dellisanti et al., 2018). The generation of these montmorillonite striations was inferred to be assisted by the presence of interlayer water, which would disappear at higher temperatures. Although chlorite lacks the interlayer water of montmorillonite, the chlorite crystal structure involves hydrophilic 2:1 talc-like sheets with a negative surface charge alternating with positively charged, hydrophobic brucite-like layers (e.g., Moro et al., 2016). Morrow et al. (2000)

showed that the tendency of chlorite to take on adsorbed water greatly reduces its strength, so these hydrophilic layers are likely to be weak at our low-temperature, fluid-saturated conditions. We therefore suggest that the presence of hydrophilic layers in the chlorite structure allows easy grain alignment which facilitates the mechanical development of striations in the slip direction at low temperature. We note a geometrical similarity with slip surface lineations that have been associated with strain weakening in quartz at 450 °C (Toy et al., 2017) and evolution from stick slip to creep in a rock analog system (Voisin et al., 2007). In those examples, however, the mechanism of lineation development involves pressure solution and thus differs from the mechanical striation development suggested in our low temperature example.

4.3. Implications for Fault Behavior

Our results indicate that the presence of chlorite may weaken and stabilize fault rocks at near-surface conditions, with the extent of this effect depending on the chlorite volume fraction (Figures 4b and 4c). Epidote and hornblende have the opposite effect; they are relatively strong and promote unstable slip. In natural faults, if a tabular zone is dominated by chlorite, slip should localize into a weak layer (Figure 1), because the chlorite is energetically favorable for deformation. We have not tested the effects of increasing slip speed to seismic velocities, and it is likely that chlorite-dominated gouges can host propagation of seismic slip, as seen in other phyllosilicates (e.g., Brantut et al., 2008; Faulkner et al., 2011). In a scenario where chlorite grows by breakdown of amphiboles at retrograde conditions, this growth may therefore allow a time-dependent variation in fault slip style, where faults are velocity-weakening until chlorite growth reaches a sufficient proportion to cause the aggregate to become velocity-strengthening.

Striated chlorite correlates with weak and stable behavior in the experiments and relatively large D_c , which is likely to mean that as soon as a striation has developed in a chlorite-dominated layer, then it is established as a weak, creeping zone. This could be a positive feedback mechanism because the weakness of the chlorite layers should encourage further alignment of chlorite grains, possibly forming boundary-parallel or S-type foliations along which shear can localize (Figures 1, 10c, and 10d; Haines et al., 2013) and thus facilitating further weakening. This feedback mechanism helps explain why striations are relatively commonly developed in phyllosilicate-rich rocks at low temperatures (Rutter et al., 1986).

The conclusion that chlorite is associated with low friction and velocity strengthening may also apply to deeper conditions. Pure chlorite is found to be weak and slide stably under almost all laboratory conditions up to 400 MPa effective stress and 600 °C (Okamoto et al., 2019). This suggests that the effect of chlorite should be to weaken and stabilize faults from greenschist conditions all the way to the surface. However, velocity-weakening could occur in some weak, phyllosilicate-rich gouges at very slow slip rates approximating plate rates (Ikari & Kopf, 2017), and in conditions where both cataclasis and pressure solution operate, relatively high sliding velocities may also induce velocity-weakening (Niemeijer & Spiers, 2007). Thus, our conclusions of added chlorite promoting fault weakness and stable sliding may not hold for certain conditions outside of those in our study or if the deformation mechanism is not brittle/frictional. Furthermore, shallow, phyllosilicate-rich faults may still host earthquake slip if high velocities are imposed by slip that nucleates elsewhere on the fault, inducing dynamic weakening mechanisms (e.g., Faulkner et al., 2011; Ujiie et al., 2013). This could lead to time-dependent variations in slip style on the same shallow fault segment (Fagereng et al., 2019). We emphasize the importance of this temporal effect in retrograde faults, where limitations of fluid availability and permeability may lead to time- and space-variable replacement of stronger, velocity-weakening minerals with weaker, velocity-strengthening chlorite or other clay minerals. Therefore, a range of fault slip styles may be seen over single earthquake cycles due to external forcing and/or over multiple earthquake cycles as the fault rock assemblage can evolve from velocity-weakening greenschist or amphibolite to a velocity-strengthening chlorite schist as a function of fluid-rock interactions (Diener et al., 2016; Schleicher et al., 2012; Wintsch et al., 1995).

5. Conclusions

We performed single-direct shear experiments on simulated fault gouges of chlorite schist, epidotite, and amphibolite end-members and mixtures at room temperature and 10 MPa normal stress. Chlorite schist has a relatively low friction coefficient of 0.36 and exhibits velocity-strengthening behavior; epidotite and amphibolite are velocity-weakening and have residual friction coefficients of 0.63 and 0.67, respectively. Adding chlorite schist to epidotite or amphibolite leads to a reduction in strength that is approximately

linearly related to the proportion of chlorite in the aggregate. Chlorite-rich slip surfaces show well-developed striations, which are not seen on epidote or hornblende-dominated slip surfaces and are weakly developed in mixtures.

The weakness of chlorite schist may be related to the mechanical development of striations, facilitated by sliding on weak, hydrophilic chlorite crystal surfaces (Morrow et al., 2000). Striation development likely lengthens grain-scale asperities in the slip direction, leading to both mechanical weakening and velocity-strengthening behavior. This is consistent with the chlorite schist exhibiting a relatively large critical slip distance compared to the epidotite. In epidotite, the generation of very fine grains while coarse crystals are preserved attests to likely wear at initially small asperity contacts, which is associated with velocity-weakening friction. Adding chlorite to epidote and amphibole disrupts the interaction at the real asperity contact areas and therefore suppresses velocity-weakening behavior.

Implications for natural faults, active at shallow depths, include that growth of chlorite, and likely other lower temperature clays, will tend to weaken and stabilize the fault. This conclusion supports the hypothesis that phyllosilicate growth in retrograde fault zones leads to progressive frictional weakening and steady fault creep. We emphasize that this effect may be time varying and relies on fluid supply to allow phyllosilicate growth. Thus, a variation of fault behaviors may arise from variable proportions of phyllosilicates and higher grade minerals in fault rocks undergoing progressive retrograde metamorphism and rehydration.

Acknowledgments

This research has received funding from the European Research Council (ERC) under the European Union's Horizon 2020 research and innovation programme (Grant Agreement 715836 "MICA" to Å. F. and Grant Agreement 714430 "PREDATORS" to M. J. I.). We thank Duncan Muir for assistance with scanning electron microscopy and Tony Oldroyd for sample preparation. Constructive reviews from Jim Evans and Marco Scuderi significantly improved the manuscript, and we also thank Associate Editor Ludmila Adam for evaluation and suggestions. All experimental data are available from the Pangaea data publisher for earth and environmental science (<https://doi.pangaea.de/10.1594/PANGAEA.914429>). The grain size data are available from the Cardiff University data repository (<https://doi.org/10.17035/d.2020.0092132507>).

References

- Abers, G. A., Mutter, C. Z., & Fang, J. (1997). Shallow dips of normal faults during rapid extension: Earthquakes in the woodlark-D'Entrecasteaux rift system, Papua New Guinea. *Journal of Geophysical Research*, *102*(B7), 15301–15317. <https://doi.org/10.1029/97JB00787>
- Apted, M. J., & Liou, J. G. (1983). Phase relations among greenschist, epidote-amphibolite, and amphibolite in a basaltic system. *American Journal of Science*, *283*-A, 328–354.
- Barth, N. C., Boulton, C., Carpenter, B. M., Batt, G. E., & Toy, V. G. (2013). Slip localization on the southern Alpine fault, New Zealand. *Tectonics*, *32*, 620–640. <https://doi.org/10.1002/tect.20041>
- Baumberger, T., & Caroli, C. (2006). Solid friction from stick-slip down to pinning and aging. *Advances in Physics*, *55*(3-4), 279–348. <https://doi.org/10.1080/00018730600732186>
- Beeler, N. M. (2007). Laboratory-observed faulting in intrinsically and apparently weak materials: Strength, seismic coupling, dilatancy, and pore-fluid pressure. In T. H. Dixon, & J. C. Moore (Eds.), *The seismogenic zone of subduction thrust faults* (pp. 370–449). New York: Columbia University Press.
- Blanpied, M. L., Marone, C. J., Lockner, D. A., Byerlee, J. D., & King, D. P. (1998). Quantitative measure of the variation in fault rheology due to fluid-rock interactions. *Journal of Geophysical Research*, *103*(B5), 9691–9712. <https://doi.org/10.1029/98JB00162>
- Boulton, C., Moore, D. E., Lockner, D. A., Toy, V. G., Townend, J., & Sutherland, R. (2014). Frictional properties of exhumed fault gouges in DFDP-1 cores, Alpine Fault, New Zealand. *Geophysical Research Letters*, *41*, 356–362. <https://doi.org/10.1002/2013GL058236>
- Boutareaud, S., Hirose, T., Andréani, M., Pec, M., Calugaru, D.-G., Boullier, A.-M., & Doan, M.-L. (2012). On the role of phyllosilicates on fault lubrication: Insight from micro- and nanostructural investigations on talc friction experiments. *Journal of Geophysical Research*, *117*, B08408. <https://doi.org/10.1029/2011JB009006>
- Brantut, N., Schubnel, A., Rouzaud, J.-N., Brunet, F., & Shimamoto, T. (2008). High-velocity frictional properties of clay-bearing fault gouge and implications for earthquake mechanics. *Journal of Geophysical Research*, *113*, B10401. <https://doi.org/10.1029/2007JB005551>
- Carpenter, B. M., Marone, C., & Saffer, D. M. (2011). Weakness of the San Andreas Fault revealed by samples from the active fault zone. *Nature Geoscience*, *4*(4), 251–254. <https://doi.org/10.1038/ngeo1089>
- Cladouhos, T. T. (1999). Shape preferred orientations of survivor grains in fault gouge. *Journal of Structural Geology*, *21*(4), 419–436. [https://doi.org/10.1016/S0191-8141\(98\)00123-0](https://doi.org/10.1016/S0191-8141(98)00123-0)
- Collettini, C., Niemeijer, A., Viti, C., & Marone, C. (2009). Fault zone fabric and fault weakness. *Nature*, *462*(7275), 907–910. <https://doi.org/10.1038/nature08585>
- Cook, N. (1981). Stiff testing machines, stick slip sliding, and the stability of rock deformation. In N. L. Carter, M. Friedman, J. M. Logan, & D. W. Stearns (Eds.), *Mechanical behavior of crustal rocks: The Handin volume, geophysical. Monograph series* (Vol. 24, pp. 93–102). Washington, DC: American Geophysical Union.
- Dellisanti, F., Calafato, A., Pini, G. A., Moro, D., Ulian, G., & Valdrè, G. (2018). Effects of dehydration and grinding on the mechanical shear behavior of Ca-rich montmorillonite. *Applied Clay Science*, *152*, 239–248. <https://doi.org/10.1016/j.clay.2017.11.019>
- Di Toro, G., Han, R., Hirose, T., De Paola, N., Nielsen, S., Mizoguchi, K., et al. (2011). Fault lubrication during earthquakes. *Nature*, *471*(7339), 494–498. <https://doi.org/10.1038/nature09838>
- Diener, J. F. A., Fagereng, Å., & Thomas, S. A. J. (2016). Mid-crustal shear zone development under retrograde conditions: Pressure–temperature–fluid constraints from the Kuckaus Mylonite zone, Namibia. *Solid Earth*, *7*, 1331–1347. <https://doi.org/10.5194/se-7-1331-2016>
- Dieterich, J. H. (1986). A model for the nucleation of earthquake slip. In S. Das, J. Boatwright, & C. H. Scholz (Eds.), *Earthquake source mechanics, Geophysical Monograph Series* (Vol. 37, pp. 37–47). Washington, DC: American Geophysical Union.
- Dieterich, J. H. (1981). Constitutive properties of faults with simulated gouge. In N. L. Carter, M. Friedman, J. M. Logan, & D. W. Stearns (Eds.), *Mechanical behavior of crustal rocks: The Handin volume, geophysical. Monograph series* (Vol. 24, pp. 103–120). Washington, DC: American Geophysical Union.
- Dieterich, J. H., & Kilgore, B. (1994). Direct observation of frictional contacts: New insights for state-dependent properties. *Pure and Applied Geophysics*, *143*(1-3), 283–302. <https://doi.org/10.1007/BF00874332>

- Dieterich, J. H., & Kilgore, B. D. (1996). Implications of fault constitutive properties for earthquake prediction. *Proceedings of the National Academy of Science*, 93(9), 3787–3794. <https://doi.org/10.1073/pnas.93.9.3787>
- Engelder, J. T. (1974). Microscopic wear grooves on slickensides, indicators of paleoseismicity. *Journal of Geophysical Research*, 79(29), 4387–4392. <https://doi.org/10.1029/JB079i029p04387>
- Evans, D. J., & White, S. H. (1984). Microstructural and fabric studies from the rocks of the Moine Nappe, Eriboll, Scotland. *Journal of Structural Geology*, 6(4), 369–389. [https://doi.org/10.1016/0191-8141\(84\)90038-5](https://doi.org/10.1016/0191-8141(84)90038-5)
- Fagereng, Å., & Diener, J. F. A. (2011). San Andreas Fault tremor and retrograde metamorphism. *Geophysical Research Letters*, 38, L23303. <https://doi.org/10.1029/2011GL049550>
- Fagereng, Å., Savage, H. M., Morgan, J. K., Wang, M., Meneghini, F., Barnes, P. M., et al., & The IODP Expedition 372/375 Scientists (2019). Mixed deformation styles observed on a shallow subduction thrust, Hikurangi margin, New Zealand. *Geology*, 47(9), 872–876. <https://doi.org/10.1130/G46367.1>
- Faulkner, D. R., Mitchell, T. M., Behnsen, J., Hirose, T., & Shimamoto, T. (2011). Stuck in the mud? Earthquake nucleation and propagation through accretionary forearcs. *Geophysical Research Letters*, 38, L18303. <https://doi.org/10.1029/2011GL048552>
- Haines, S. H., Kaproth, B., Marone, C., Saffer, D., & van der Pluijm, B. (2013). Shear zones in clay-rich fault gouge: A laboratory study of fabric development and evolution. *Journal of Structural Geology*, 51, 206–225. <https://doi.org/10.1016/j.jsg.2013.01.002>
- Hancock, P. L. (1985). Brittle microtectonics: Principles and practice. *Journal of Structural Geology*, 7(3-4), 437–457. [https://doi.org/10.1016/0191-8141\(85\)90048-3](https://doi.org/10.1016/0191-8141(85)90048-3)
- Heilbronner, R. (2000). Automatic grain boundary detection and grain size analysis using polarization micrographs or orientation images. *Journal of Structural Geology*, 22(7), 969–981.
- Holdsworth, R. E., Alsop, G. I., & Strachan, R. A. (2007). Tectonic stratigraphy and structural continuity of the northernmost Moine thrust zone and Moine Nappe, Scottish Caledonides. *Geological Society, London, Special Publications*, 272(1), 121–142. <https://doi.org/10.1144/GSL.SP.2007.272.01.08>
- Holdsworth, R. E., van Diggelen, E. W. E., Spiers, C. J., de Bresser, J. H. P., Walker, R. J., & Bowen, L. (2011). Fault rocks from the SAFOD core samples: Implications for weakening at shallow depths along the San Andreas Fault, California. *Journal of Structural Geology*, 33(2), 132–144. <https://doi.org/10.1016/j.jsg.2010.11.010>
- Ikari, M. J., Carpenter, B. M., & Marone, C. (2016). A microphysical interpretation of rate- and state-dependent friction for fault gouge. *Geochemistry, Geophysics, Geosystems*, 17(5), 1660–1677. <https://doi.org/10.1002/2016GC006286>
- Ikari, M. J., Ito, Y., Ujiie, K., & Kopf, A. J. (2015). Spectrum of slip behaviour in Tohoku fault zone samples at plate tectonic slip speeds. *Nature Geoscience*, 8(11), 870–874. <https://doi.org/10.1038/ngeo2547>
- Ikari, M. J., & Kopf, A. J. (2011). Cohesive strength of clay-rich sediment. *Geophysical Research Letters*, 38, L16309. <https://doi.org/10.1029/2011GL047918>
- Ikari, M. J., & Kopf, A. J. (2017). Seismic potential of weak, near-surface faults revealed at plate tectonic slip rates. *Science Advances*, 3(11), e1701269. <https://doi.org/10.1126/sciadv.1701269>
- Ikari, M. J., Marone, C., & Saffer, D. M. (2011). On the relation between fault strength and frictional stability. *Geology*, 39(1), 83–86. <https://doi.org/10.1130/G31416.1>
- Ikari, M. J., Saffer, D. M., & Marone, C. (2009). Frictional and hydrologic properties of clay-rich fault gouge. *Journal of Geophysical Research*, 114, B05409. <https://doi.org/10.1029/2008JB0066089>
- Ikari, M. J., Trütner, S., Carpenter, B. M., & Kopf, A. J. (2015). Shear behavior of DFDP-1 borehole samples from the Alpine Fault, New Zealand under a wide range of experimental conditions. *International Journal of Earth Sciences*, 104(6), 1523–1535. <https://doi.org/10.1007/s00531-014-1115-5>
- Imber, J., Holdsworth, R. E., Butler, C. A., & Lloyd, G. E. (1997). Fault-zone weakening processes along the reactivated outer Hebrides fault zone, Scotland. *Journal of the Geological Society*, 154(1), 105–109. <https://doi.org/10.1144/gsjgs.154.1.0105>
- Imber, J., Holdsworth, R. E., Butler, C. A., & Strachan, R. A. (2001). A reappraisal of the Sibson-Scholz fault zone model: The nature of the frictional to viscous ('brittle-ductile') transition along a long-lived, crustal-scale fault, outer Hebrides, Scotland. *Tectonics*, 18, 326–342.
- Ito, Y., & Ikari, M. J. (2015). Velocity- and slip-dependent weakening in simulated fault gouge: Implications for multimode fault slip. *Geophysical Research Letters*, 42, 9247–9254. <https://doi.org/10.1002/2015GL065829>
- Jefferies, S. P., Holdsworth, R. E., Wibberley, C. A. J., Shimamoto, T., Spiers, C. J., Niemeijer, A. R., & Lloyd, G. E. (2006). The nature and importance of phyllonite development in crustal-scale fault cores: An example from the median tectonic line, Japan. *Journal of Structural Geology*, 28(2), 220–235. <https://doi.org/10.1016/j.jsg.2005.10.008>
- Jiang, J., & Lapusta, N. (2017). Connecting depth limits of interseismic locking, microseismicity, and large earthquakes in models of long-term fault slip. *Journal of Geophysical Research*, 122, 6491–6523. <https://doi.org/10.1002/2017JB014030>
- Jiménez-Millán, J., Abad, I., Hernández-Puentes, P., & Jiménez-Espinoza, R. (2015). Influence of phyllosilicates and fluid–rock interaction on the deformation style and mechanical behaviour of quartz-rich rocks in the Carboneras and Palomares fault areas (SE Spain). *Clay Minerals*, 50(5), 619–638. <https://doi.org/10.1180/claymin.2015.050.5.06>
- Logan, J. M., & Rauenzahn, K. A. (1987). Frictional dependence of gouge mixtures of quartz and montmorillonite on velocity, composition, and fabric. *Tectonophysics*, 144(1-3), 87–108. [https://doi.org/10.1016/0040-1951\(87\)90010-2](https://doi.org/10.1016/0040-1951(87)90010-2)
- Marone, C. (1998). Laboratory-derived friction laws and their application to seismic faulting. *Annual Review of Earth and Planetary Sciences*, 26(1), 643–696. <https://doi.org/10.1146/annurev.earth.26.1.643>
- Marone, C., Raleigh, C. B., & Scholz, C. H. (1990). Frictional behavior and constitutive modeling of simulated fault gouge. *Journal of Geophysical Research*, 95(B5), 7007–7025. <https://doi.org/10.1029/JB095iB05p07007>
- McClay, K. R., & Coward, M. P. (1981). The Moine thrust zone: An overview. *Geological Society of London, Special Publication*, 9(1), 241–260. <https://doi.org/10.1144/GSL.SP.1981.009.01.22>
- Miyashiro, A. (1968). Metamorphism of mafic rocks. In H. H. Hess, & A. Poldervaart (Eds.), *Basalts* (pp. 799–834). New York: John Wiley & Sons.
- Mori, Y., Shigeno, M., & Nishiyama, T. (2014). Fluid-metapelite interaction in an ultramafic mélange: Implications for mass transfer along the slab-mantle interface in subduction zones. *Earth, Planets and Space*, 66(1), 47. <https://doi.org/10.1186/1880-5981-66-47>
- Moro, D., Ulian, G., & Valdrè, G. (2016). Nanoscale cross-correlated AFM, kelvin probe, elastic modulus and quantum mechanics investigation of clay mineral surfaces: The case of chlorite. *Applied Clay Science*, 131, 175–181. <https://doi.org/10.1016/j.clay.2015.11.023>
- Morrow, C. A., Moore, D. E., & Lockner, D. A. (2000). The effect of mineral bond strength and adsorbed water on fault gouge frictional strength. *Geophysical Research Letters*, 27(6), 815–818. <https://doi.org/10.1029/1999GL008401>

- Morrow, C. A., Radney, B., & Byerlee, J. (1992). Frictional strength and the effective pressure law of montmorillonite and illite clays. In B. Evans & T.-F. Wong (Eds.), *Fault Mechanics and Transport Properties of Rocks* (pp. 69–88). London: Academic Press.
- Niemeijer, A. R., Boulton, C., Toy, V. G., Townend, J., & Sutherland, R. (2016). Large-displacement, hydrothermal frictional properties of DFDP-1 fault rocks, Alpine Fault, New Zealand: Implications for deep rupture propagation. *Journal of Geophysical Research - Solid Earth*, *121*(2), 624–647. <https://doi.org/10.1002/2015JB012593>
- Niemeijer, A. R., & Spiers, C. J. (2005). Influence of phyllosilicates on fault strength in the brittle-ductile transition: Insights from rock analogue experiments. *Geological Society, London, Special Publications*, *245*(1), 303–327. <https://doi.org/10.1144/GSL.SP.2005.245.01.15>
- Niemeijer, A. R., & Spiers, C. J. (2007). A microphysical model for strong velocity weakening in phyllosilicate-bearing gouges. *Journal of Geophysical Research*, *112*, B10405. <https://doi.org/10.1029/2007JB005008>
- Norris, R. J., & Cooper, A. F. (2007). The Alpine fault, New Zealand: Surface geology and field relationships. In D. Okaya, T. Stern, & F. Davey (Eds.), *A continental plate boundary: Tectonics at South Island* (Vol. 175, pp. 157–175). New Zealand: American Geophysical Union Monograph. <https://doi.org/10.1029/175GM09>
- Okamoto, A. S., Verberne, B. A., Niemeijer, A. R., Takahashi, M., Shimizu, I., Ueda, T., & Spiers, C. J. (2019). Frictional properties of simulated chlorite gouge at hydrothermal conditions: Implications for subduction megathrusts. *Journal of Geophysical Research*, *124*, 4545–4565. <https://doi.org/10.1029/2018JB017205>
- Petit, J. P. (1987). Criteria for the sense of movement on fault surfaces in brittle rocks. *Journal of Structural Geology*, *9*(5–6), 597–608. [https://doi.org/10.1016/0191-8141\(87\)90145-3](https://doi.org/10.1016/0191-8141(87)90145-3)
- Read, H. H. (1934). Age problems in the Moine series of Scotland. *Geological Magazine*, *71*(7), 302–317. <https://doi.org/10.1017/S0016756800093389>
- Reinen, L. A., & Weeks, J. D. (1993). Determination of rock friction constitutive parameters using an iterative least squares method. *Journal of Geophysical Research*, *98*(B9), 15937–15950. <https://doi.org/10.1029/93JB00780>
- Richard, J., Gratier, J.-P., Doan, M.-L., Boullier, A.-M., & Renard, F. (2014). Rock and mineral transformations in a fault zone leading to permanent creep: Interactions between brittle and viscous mechanisms in the San Andreas Fault. *Journal of Geophysical Research*, *119*, 8132–8153. <https://doi.org/10.1002/2014jb011489>
- Rutter, E. H., Hackston, A. J., Yeatman, E., Brodie, K. H., Mecklenburgh, J., & May, S. E. (2013). Reduction of friction on geological faults by weak-phase smearing. *Journal of Structural Geology*, *51*, 52–60. <https://doi.org/10.1016/j.jsg.2013.03.008>
- Rutter, E. H., Maddock, R. H., Hall, S. H., & White, S. H. (1986). Comparative microstructures of natural and experimentally produced clay-bearing fault gouges. *Pure and Applied Geophysics*, *124*(1–2), 3–30. <https://doi.org/10.1007/BF00875717>
- Saffer, D. M., & Marone, C. (2003). Comparison of smectite- and illite-rich gouge frictional properties: Application to the updip limit of the seismogenic zone along subduction megathrusts. *Earth and Planetary Science Letters*, *215*(1–2), 219–235. [https://doi.org/10.1016/S0012-821X\(03\)00424-2](https://doi.org/10.1016/S0012-821X(03)00424-2)
- Sánchez-Roa, C., Faulkner, D. R., Boulton, C., Jimenez-Millan, J., & Nieto, F. (2017). How phyllosilicate mineral structure affects fault strength in mg-rich fault systems. *Geophysical Research Letters*, *44*, 5457–5467. <https://doi.org/10.1002/2017GL073055>
- Schleicher, A. M., van der Pluijm, B. A., & Warr, L. (2012). Chlorite-smectite clay minerals and fault behavior: New evidence from the San Andreas Fault Observatory at Depth (SAFOD) core. *Lithosphere*, *4*(3), 209–220. <https://doi.org/10.1130/L158.1>
- Scholz, C. H. (1998). Earthquakes and friction laws. *Nature*, *391*(6662), 37–42. <https://doi.org/10.1038/34097>
- Scruggs, V. J., & Tullis, T. E. (1998). Correlation between velocity dependence of friction and strain localization in large displacement experiments on feldspar, muscovite and biotite gouge. *Tectonophysics*, *295*(1–2), 15–40. [https://doi.org/10.1016/S0040-1951\(98\)00113-9](https://doi.org/10.1016/S0040-1951(98)00113-9)
- Scuderi, M. M., Collettini, C., Viti, C., Tinti, E., & Marone, C. (2017). Evolution of shear fabric in granular fault gouge from stable sliding to stick slip and implications for fault slip mode. *Geology*, *45*, 731–734.
- Segall, P., & Rice, J. R. (2006). Does shear heating of pore fluid contribute to earthquake nucleation? *Journal of Geophysical Research*, *111*, B09316. <https://doi.org/10.1029/2005JB004129>
- Shimamoto, T., & Logan, J. M. (1981a). Effects of simulated fault gouge on the sliding behavior of Tennessee sandstone: Nonclay gouges. *Journal of Geophysical Research*, *86*, 2902–2914. <https://doi.org/10.1029/JB086iB04p02902>
- Shimamoto, T., & Logan, J. M. (1981b). Effects of simulated clay gouges on the sliding behavior of Tennessee sandstone. *Tectonophysics*, *75*(3–4), 243–255. [https://doi.org/10.1016/0040-1951\(81\)90276-6](https://doi.org/10.1016/0040-1951(81)90276-6)
- Shimamoto, T., & Nagahama, H. (1992). An argument against the crush origin of pseudotachylytes based on the analysis of clast-size distributions. *Journal of Structural Geology*, *14*(8–9), 999–1006. [https://doi.org/10.1016/0191-8141\(92\)90031-Q](https://doi.org/10.1016/0191-8141(92)90031-Q)
- Sibson, R. H. (1982). Fault zone models, heat flow, and the depth distribution of earthquakes in the continental crust of the United States. *Bulletin of the Seismological Society of America*, *72*, 151–163.
- Sleep, N. H. (2005). Physical basis of evolution laws for rate and state friction. *Geochemistry, Geophysics, Geosystems*, *6*, Q11008. <https://doi.org/10.1029/2005GC000991>
- Smith, S. A. F., & Faulkner, D. R. (2010). Laboratory measurements of the frictional properties of the Zuccale low-angle normal fault, Elba Island, Italy. *Journal of Geophysical Research*, *115*, B02407. <https://doi.org/10.1029/2008JB006274>
- Taylor, B., & Huchon, P. (2002). Active continental extension in the western Woodlark Basin: A synthesis of leg 180 results. In P. Huchon, B. Taylor, & A. Klaus (Eds.), *Proc. ODP, Sci. Results*, *180*, (pp. 1–36). College Station: TX (ocean drilling program). <https://doi.org/10.2973/odp.proc.sr.180.150.2002>
- Taylor, B., Huchon, P., Klaus, A., et al. (2000). *Proc. ocean drill. Program, initial rep.*, 190. College Station: TX (ocean drilling program). <https://doi.org/10.2973/odp.proc.ir.180.2000>
- Tesei, T., Collettini, C., Carpenter, B. M., Viti, C., & Marone, C. (2012). Frictional strength and healing behavior of phyllosilicate-rich faults. *Journal of Geophysical Research*, *117*, B09402. <https://doi.org/10.1029/2012JB009204>
- Toy, V. G., Boulton, C. J., Sutherland, R., Townend, J., Norris, R. J., Little, T. A., et al. (2015). Fault rock lithologies and architecture of the Central Alpine fault, New Zealand, revealed by DFDP-1 drilling. *Lithosphere*, *7*(2), 155–173. <https://doi.org/10.1130/L395.1>
- Toy, V. G., Niemeijer, A., Renard, F., Morales, L., & Wirth, R. (2017). Striation and slickenline development on quartz fault surfaces at crustal conditions: Origin and effect on friction. *Journal of Geophysical Research*, *122*, 3497–3512. <https://doi.org/10.1002/2016JB013498>
- Ujiie, K., Tanaka, H., Saito, T., Tsutsumi, A., Mori, J. J., Kameda, J., et al., & Expedition 343 and 343T Scientists (2013). Low coseismic shear stress on the Tohoku-Oki megathrust determined from laboratory experiments. *Science*, *342*(6163), 1211–1214. <https://doi.org/10.1126/science.1243485>
- Vogt, C., Lauterjung, J., & Fischer, R. (2002). Investigation of the clay fraction (<2 μm) of the clay minerals society reference clays. *Clays and Clay Minerals*, *50*(3), 388–400. <https://doi.org/10.1346/000986002760833765>

- Voisin, C., Renard, F., & Grasso, J.-R. (2007). Long term friction: From stick-slip to stable sliding. *Geophysical Research Letters*, *34*, L13301. <https://doi.org/10.1029/2007gl029715>
- Wintsch, R. P., Christoffersen, R., & Kronenberg, A. K. (1995). Fluid-rock reaction weakening of fault zones. *Journal of Geophysical Research*, *100*, 13021–13032. <https://doi.org/10.1029/94jb02622>
- Zwaan, K. B., & Roberts, D. (1978). Tectonostratigraphic succession and development of the Finnmarkian nappe sequence, North Norway. *Norges Geologiske Undersøkelse*, *343*, 53–71.